Astronomical & Astrophysical Transactions
The Journal of the Eurasian Astronomical Society

Deuterium to hydrogen towards QSO 1009 2956 from a mesoturbulent model

S. A. Levshakov [a]; D. Tytler [b]; S. Burles [c]
[a] Department of Theoretical Astrophysics, Ioffe Physico-Technical Institute, St Petersburg, Russia
[b] Department of Physics and Centre for Astrophysics and Space Sciences, University of California, CA
[c] University of Chicago, Chicago, IL

PLEASE SCROLL DOWN FOR ARTICLE

DEUTERIUM TO HYDROGEN TOWARDS QSO 1009+2956 FROM A MESOTURBULENT MODEL[†]

S. A. LEVSHAKOV[1], D. TYTLER[2], and S. BURLES[3]

[1]*Department of Theoretical Astrophysics, Ioffe Physico-Technical Institute, 194021, St Petersburg, Russia*

[2]*Department of Physics and Centre for Astrophysics and Space Sciences, University of California, San Diego, MS 0424, La Jolla, CA 92093-0424*

[3]*University of Chicago, 5640 S. Ellis Ave., Chicago, IL 60637*

We present a new analysis of the deuterium absorption at $z = 2.504$ towards the quasar Q1009+2956 using the mesoturbulent model which accounts for possible correlations in the large-scale velocity field. We obtain a slightly higher deuterium-to-hydrogen ratio $D/H \simeq (3.5–5.0) \times 10^{-5}$ as compared with the recent measurement $D/H \simeq (3.3–4.5) \times 10^{-5}$ (68% C.L.) performed by Burles and Tytler (1998b) using the usual microturbulent approximation which assumes that the velocity field is uncorrelated. Other mesoturbulent calculations of the D-abundances at $z = 3.572$ towards Q1937−1009 and at $z = 0.701$ towards Q1718+4807 (the systems showing 'low' and possibly 'high' D/H values, respectively, in the microturbulent approaches) agree with the present one within the errors of measurements. Thus, the mesoturbulent analysis does not reveal any spatial variations of D/H and supports the standard homogeneous model of big bang nucleosynthesis.

KEY WORDS   Big Bang nucleosynthesis, quasars, deyterium abundances, QSO 1009+2956

1   INTRODUCTION

High-resolution spectra of the H + D absorption in Lyman limit systems towards distant quasars and the subsequent Voigt profile fitting analysis (VPF) suggested a dispersion in the primordial hydrogen isotopic ratio $D/H \equiv N(D\ I)/N(H\ I)$ (the ratio of the D I and H I column densities) of about one order of magnitude (see a short summary in Burles and Tytler, 1998b; BT hereinafter). This finding provoked a lively discussion in the literature on inhomogeneous models of big bang nucleosynthesis (e.g., Jedamzik and Fuller, 1995; Webb *et al.*, 1997; Kurki-Suonio *et al.*, 1997). The standard (homogeneous) BBN predicts the same D/H abundance

---

[†]Based on observations obtained at the W. M. Keck Observatory, which is jointly operated by the University of California and the California Institute of Technology.

ratios in different directions in the early Universe since 'no realistic astrophysical process other than the Big Bang could produce significant D' (Schramm, 1998, p.6). Deuterium is created exclusively in BBN and therefore we can expect that the D/H ratio decreases with cosmic time due to conversion of D into ^{3}He and heavier elements in stars. It is clear that the precise measurements of the D/H values at high redshift are extremely important to probe whether BBN was homogeneous. The choice of the appropriate BBN model may in turn place constrains on different models of structure formation.

In spectral analysis we never know exactly the line formation process. The lack of information about the nature of the absorption line broadening mechanism means that we might obtain different values of D/H if we make different assumptions. The multicomponent microturbulent models which are normally used assume that the apparent fluctuations within the line profile are caused by the density clumps ('cloudlets') with different radial velocities. The thermal and non-thermal (turbulent) velocities inside each cloudlet are assumed to be represented by plain Gaussian distributions with the total velocity dispersion being

$$b_{obs}^2 = b_{therm}^2 + b_{turb}^2. \tag{1}$$

By contrast, the mesoturbulent approach is based on the assumption that the intensity fluctuations within the line profile arise mainly from the irregular Doppler shifts in the absorption coefficient caused by macroscopic large-scale, rather than thermal, motions. Large-scale velocity fields suggest immanent coherent (correlated) structures. If the macroscopic velocity field has a correlation length not small as compared with the linear size of the absorbing region, then the radial velocity distribution may deviate significantly from the Gaussian model. The relationship (1) is then no longer valid and we cannot interpret the apparent line width in terms of b_{therm} and b_{turb}. To estimate the thermal and turbulent velocities stochastic optimization procedures are to be used in this case. The application of the standard VPF analysis to complex profiles caused by the large-scale velocity flows may give incorrect physical parameters (Levshakov, Kegel and Mazets, 1997; Paper II hereinafter). We do not know, however, how to distinguish between the multicomponent microturbulent and one-component mesoturbulent models if both of them show good fits to the spectral data.

To decide which model is better additional observations can be considered. For instance, if we assume that the Lyman limit systems arise in the outer regions of intervening galactic halos, then direct observations of the large-scale flows in the giant Lyα emission halos at $z > 2$ (van Ojik *et al.*, 1997), or in the star-forming galaxies at $z \simeq 3$ (Pettini *et al.*, 1998), or the complex metal absorption-line features in the quasar absorber/galaxy pairs at $z \sim 1$ (Bergeron *et al.*, 1992; Bechtold and Ellingson, 1992; Charlton and Churchill, 1998) may favour the mesoturbulent approximation since the rms turbulent velocity ($\sigma_t \equiv b_{turb}/\sqrt{2}$) in these halos ($\sigma_t \sim$ 20–100 km s^{-1}) is larger that the thermal width ($v_{th} \equiv b_{therm}$) of the hydrogen lines ($v_{th} \sim$ 13–15 km s^{-1}). The correlation effects become important if $\sigma_t/v_{th} \gtrsim 1$. Examples are given in Paper II.

The first D/H measurement at $z = 2.504$ towards Q1009+2956 was performed by Tytler and Burles (1997). They found D/H in the range from 2.2×10^{-5} to 4.2×10^{-5}. Later BT reconsidered this measurement including full coverage of the Lyman series and better quality data above and below the Lyman continuum break. Besides BT used the new method to measure D/H in quasar absorption systems described in Burles and Tytler (1998a). Considering six different microturbulent models, BT found D/H = $(3.9 \pm 0.6) \times 10^{-5}$ which is consistent with their results on the $z = 3.572$ system towards Q1937−1009 where D/H = $(3.3 \pm 0.3) \times 10^{-5}$ (Burles and Tytler, 1998a). Neither measurement is consistent with the D/H at $z = 0.701$ towards Q1718+4807 deduced using the microturbulent model with a single component: D/H = $(2.0 \pm 0.5) \times 10^{-4}$ (Webb et al., 1997), and $8 \times 10^{-5} <$ D/H $< 57 \times 10^{-5}$ (Tytler et al., 1998). This discord can be resolved using a more complex velocity model for Q1718+4807. For example, Tytler et al. (1998) considered a second velocity component within the microturbulent model, while Levshakov et al. (1998b) used a mesoturbulent model. Since we cannot decide a priori which mechanism − density fluctuations or large-scale velocity field − is responsible for the observed complexity of the line profiles, it is reasonable to analyse data by both micro- and mesoturbulent procedures to check the validity of the D/H measurements.

Here we apply the mesoturbulent model to Q1009+2956, and we conclude that the mesoturbulent approach allows us to describe H + D profiles in the three foregoing QSO systems by a single value of D/H which is approximately equal to 4×10^{-5}.

2 THE MEASUREMENT OF D/H

The present study is primarily aimed at the inverse problem in the analysis of the H + D Lyα absorption. The higher-order Lyman series lines observed by BT (Lyβ, Ly-6, Ly-12, Ly-13, Ly-14, Ly-20, and Ly-21) were also chosen in this analysis to restrict the set of possible velocity field configurations. We consider an absorbing region of thickness L which is a continuous medium (presumably the outer region of a foreground galaxy). The absorber is assumed to exhibit a mixture of bulk motions such as infall and outflows, tidal flows, etc. Then the motion along the sight-line may be characterized by a fluctuating velocity field that we consider as a continuous random function of the space coordinate, $v(s)$.

For simplicity, we assume a homogeneous density n_e and temperature T_{kin}. We have only weak justifications for these assumptions, which are necessitated by the complexity of the analysis. The assumption of constant T_{kin} may be supported by the fact that the states of thermally stable, optically thin interstellar gas take only restricted temperature ranges over a relatively wide range of density variations (see Donahue and Shull, 1991; DS hereinafter). In this paper we consider T_{kin} as being the mean kinetic temperature along the line of sight.

The constant n_e seems to be a quite plausible approximation for this particular $z = 2.504$ system since observational data show that metal lines from different ions show similar profiles, i.e. they arise in the same volume elements. In Section 3 we
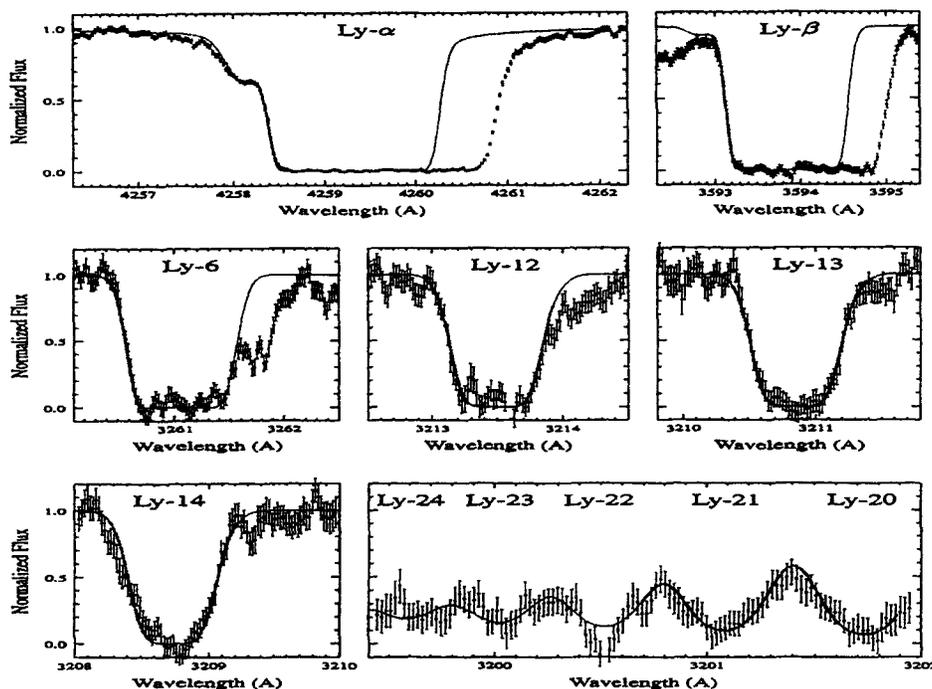
Figure 1 Observations (normalized flux) and RMC fits for Q1009+2956. The Keck/HIRES echelle data obtained by BT – dots and 1σ error bars; the calculated RMC profiles (model (a) in Table 2) convolved with the instrumental resolution of FWHM $= 8$ km s^{-1} – solid curves. The thicker grey parts of these curves show the regions about each Lyman line used in the fitting procedure. The redshift of this Lyman limit system is $z = 2.503571$, according to BT.

use the similarity of C IV and Si IV profiles to estimate $T_{\rm kin}$ independently on the analysis of hydrogen lines. But these arguments do not rule out possible variations in $T_{\rm kin}$ and/or n_e in general. Our present mesoturbulent model is similar to that adopted in Levshakov *et al.* (1998a, 1998b).

We have developed a computational procedure which allows us to estimate physical parameters and simultaneously an appropriate velocity field structure along the sight-line. The details of the computational scheme based on the reverse Monte-Carlo technique (RMC) are given in Levshakov *et al.* (1999a, Paper III hereinafter). The algorithm requires us to define a simulation box for the parameter vector $\theta = \{{\rm D/H}, {\rm N(H~I)}, T_{\rm kin}, \sigma_t/v_{\rm th}, L/l\}$; here l is the velocity field correlation length. The continuous random function $v(s)$ is represented by its sampled values at equal space intervals Δs, i.e. by the sequence v_j $(j = 1, 2, \ldots, k)$ of the velocity components parallel to the line of sight at the spatial points s_j. We describe v_j by a two-point Markovian process.

In the present study we adopt for the physical parameters the following boundaries: N(H I) ranges from 2.0×10^{17} to 3.0×10^{17} cm^{-2} – the total hydrogen column

density measured from the Lyman continuum optical depth by BT was found to lie in the interval $(2.1-2.8) \times 10^{17}$ cm^{-2}; D/H – from 3.0×10^{-5} to 3.0×10^{-4}; T_{kin} – from 10^4 to 2.5×10^4 K. For σ_t/v_{th} the boundaries were set from 1.0 to 2.5 to be typical for that observed in galactic halos. Since for $L/l \gg 1$ the meso- and microturbulent profiles tend to be identical (Levshakov and Kegel, 1997; Paper I hereinafter), we consider here only moderate L/l ratios in the range 1–5. We do not assume that the D and H lines have identical velocities to the metal lines. The H I distribution is restricted by the higher-order Lyman series lines. We fix $z = 2.503571$ (the value adopted by BT) as the reference radial velocity at which $v = 0$.

We use a χ^2 minimization routine and the RMC optimization technique to esti- mate five model parameters and the appropriate configuration of the velocity field $v(s)$. Note that k components of the velocity field here are the 'nuisance parame- ters' and their number does not influence the physical parameters we are interested in. A lower bound to k is given by the inequality (Eq. (22) in Paper II):

$$\frac{L}{\Delta s} > \frac{L}{l} \frac{2}{\ln[1 - (v_{th}/\sigma_t)^2]^{-1}}, \tag{2}$$

with $\sigma_t/v_{th} > 1$.

In the Q1009+2956 spectrum, there are many absorption features blending the Lyman series lines. We do not fit these additional absorptions since they do not affect significantly the D/H measurement in this system, as shown by BT. The strongest absorption feature seen at $z = 2.50456$ in Figure 1 has, according to BT, N(H I) $= 3.7 \times 10^{13}$ cm^{-2}, which is less than 0.02% of the total N(H I) at $z = 2.504$.

The portions of the Lyman series lines that, after preliminary analysis, were chosen as most appropriate to the simultaneous RMC fitting are indicated in Figure 1 by the thick grey lines. In the standard χ^2 minimization, the following objective function is usually used

$$\mathcal{L} \equiv \chi^2 = \frac{1}{\nu} \sum_{j=1}^{n} \sum_{i=1}^{m_j} \frac{[I_i - F(\lambda_i, \theta)]^2}{\sigma_{I_i}^2}. \tag{3}$$

Here, I_i and σ_{I_i}, are the observed normalized intensity and the experimental error within the ith pixel of the line profile, respectively. $F(\lambda_i, \theta)$ is the simulated in- tensity at the same ith pixel having wavelength λ_i. The total number of hydrogen lines is labelled by n, and the total number of data points $m = \sum_{j=1}^{n} m_j$, where m_j is the number of data points for the jth line. The number of fitted parameters is $p = 5$, and $\nu = m - p$ is the degrees of freedom ($\nu = 208$ in our case).

Equation (3) assumes that all λ_i-values are known exactly, and thus it ignores errors in the wavelength calibrations (λ-errors). These errors can be neglected in the case of not very steep profiles and not very high signal-to-noise (SNR) data, when small errors in λ leave the intensity within its uncertainty range, i.e.

$$I + \left| \frac{dI}{d\lambda} \right| \sigma_\lambda < I + \sigma_I,$$

Table 1. H I data for the λ-adjustment criterion (Eq. (4)).

	Lyα	*Lyβ*	*Ly-6*	*Ly-12*
$\lambda\lambda$, Å	4258.30–4258.50	3593.01–3593.21	3260.50–3260.66	3213.03–3213.21
$\langle SNR \rangle$	80	36	17	13
σ_I/σ_λ, Å^{-1}	0.4	1.0	3.0	4.0
$dI/d\lambda$, Å^{-1}	3.0	4.0	5.0	4.0

or

$$\left| \frac{dI}{d\lambda} \right| < \frac{\sigma_I}{\sigma_\lambda}, \tag{4}$$

where $\sigma_\lambda = (\sigma_{stat}^2 + \sigma_{system}^2)^{1/2}$ is the error of the wavelength scale calibration, and σ_I is the experimental uncertainty in I.

If, however, inequality (4) is violated, then the calibration errors, appearing in the shift of the line profile, lead to inappropriate high values of $\mathcal{L}$. To correct such solutions, we should adjust the λ scale. We have calculated (4) for different lines under consideration (see Table 1). From this table it is seen that (4) is strongly violated for the Lyα, Lyβ and Ly-6 lines, but is satisfied for the Ly-12 and higher-order hydrogen lines.

To account for the λA-adjustment we incorporate new fitting parameters $\delta\lambda$ in equation (3) which now takes the form

$$\chi^2 = \frac{1}{\nu'} \left\{ \sum_{j=1}^{n} \sum_{i=1}^{m_j} \frac{[I_i - F(\lambda_i + \delta\lambda_j, \theta)]^2}{\sigma_{I_i}^2} + \sum_{j=1}^{n'} \left(\frac{\delta\lambda_j}{\sigma_{\lambda_j}} \right)^2 \right\}, \tag{5}$$

where the correction factor $\delta\lambda_j$ is common for all pixels of the jth hydrogen line. n' is the number of lines whose wavelength scales are to be corrected $(0 \leq n' \leq n)$, and $\sigma_{\lambda_j} \equiv \sigma_\lambda \simeq (1/4)$FWHM. The number of fitted parameters in this case is $p' = 5 + n'$ and hence $\nu' = m - p'$. In this approach possible values of $\delta\lambda_j$ are restricted and lie in the range $|\delta\lambda_j| < \sigma_\lambda$.

Using the original continuum as determined by BT (without allowing for errors in the local continuum in the vicinity of each hydrogen line) we found a few RMC profile fits which are listed in Table 2. We tried to find solutions with the reduced χ^2 per degree of freedom of $\chi_{min}^2 \lesssim 1$. For all models from Table 2 the calculated hydrogen profiles are similar to that shown in Figure 1. We do not find any large differences between calculated and real spectra. The under-absorption on the blue-ward side of D Lyα is probably caused by the Lyα forest lines. We do not treat this part of the spectrum because, in this case, unsaturated higher-order Lyman series lines provide accurate predictions for the velocity of the deuterium Lyα line and its shape. Besides, as shown by BT, these additional absorptions do not affect significantly the D/H ratio in the $z = 2.504$ system.

The derived $v(s)$ configurations are not unique. But their projections – the radial-velocity distribution functions $p(v)$ – are very much alike. Figure 2 shows the

Table 2. Model parameters derived from the Lyman series lines by the RMC method.

Model	D/H	N_{17}	T_4	σ_t/v_{th}	L/l	χ^2_{min}	$\delta\lambda_\alpha$	$\delta\lambda_\beta$	$\delta\lambda_6$
(a)	3.76	2.37	1.38	1.75	2.03	0.80	0.018	−0.019	−0.022
(b)	4.26	2.17	1.81	1.18	2.18	0.84	0.028	−0.014	−0.022
(c)	4.34	2.20	1.57	2.00	1.68	0.73	0.021	−0.013	−0.022
(d)	4.37	2.20	1.55	1.58	2.17	0.73	0.026	−0.011	−0.022
(e)	4.39	2.16	1.51	1.58	1.65	0.72	0.023	−0.014	−0.022
(f)	4.51	2.19	1.64	1.09	2.03	0.83	0.023	−0.015	−0.022
(g)	4.65	2.15	1.37	1.17	3.70	0.71	0.026	−0.011	−0.022

Note : N_{17} is the total hydrogen column density in units of 10^{17} cm^{-2}, D/H in units of 10^{-5}, T_4 kinetic temperature in units of 10^4 K, $\delta\lambda_j$ adjustment factor in Å, where $\delta\lambda_\alpha$, $\delta\lambda_\beta$, and $\delta\lambda_6$ are the wavelength corrections for Lyα, Lyβ, and Ly-6, respectively.
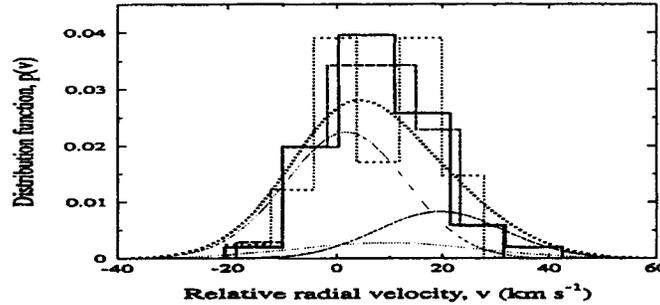

Figure 2 Radial-velocity distribution functions $p(v)$ of the RMC solutions for models (a), (e), and (g) (solid, dashed and dotted line histograms, respectively) and for comparison three $p(v)$ distributions with the velocity dispersions $b(H) = 16.0$, 16.8, and 24.6 km s^{-1} (solid curves) adopted from the best fit microturbulent model 2 of BT. The curves are weighted by the corresponding hydrogen column densities of 1.29×10^{17}, 0.50×10^{17} and 0.24×10^{17} cm^{-2}. The sum of all three weighted functions is shown by the dotted curve.

$p(v)$ distributions found by the RMC procedure (histograms) and for comparison $p(v)$ for the best three-component microturbulent model 2 found by BT (the *thin-line* are Gaussians and their weighted sum is shown by the *dotted-line*). Both the RMC $p(v)$ and the combined BT $p(v)$ distributions show similar asymmetry. But the interpretation of these $p(v)$ is different. In the microturbulent model the asymmetry is caused by the individual clouds with different physical parameters, whereas the mesoturbulent solution describes the homogeneously distributed gas with constant density and temperature along the sight-line. The fact that for this particular case the micro- and mesoturbulent distribution functions $p(v)$ are found to be similar implies that the column densities N(H I) and N(D I) should be approximately the same as well. By this, we confirm the D/H value found by BT at $z = 2.504$ towards Q1009+2956.
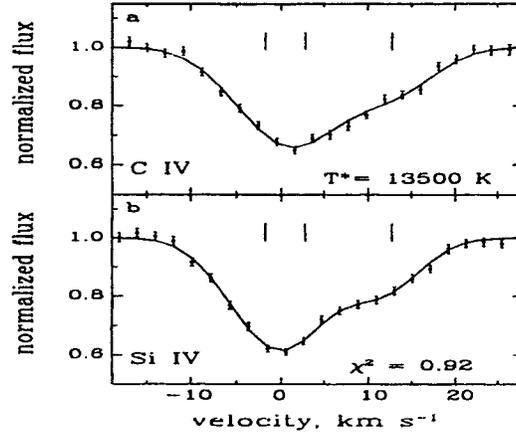
Figure 3 (*a*, *b*) Normalized data points with 1σ error bars for HIRES echelle spectrograph observations (FWHM $=$ 8 km s^{-1}) on the Keck telescope of the C IVλ1548 (SNR $=$ 72) and Si IVλ1394 (SNR $=$ 73) at the redshift $z =$ 2.503571 towards the quasar Q1009+2956 (BT). The ERM result (reduced $\chi^2 =$ 0.92 with 37 degrees of freedom) for C IV and Si IV (solid lines) is based on simultaneously fitting the multiple equidispersion lines located at the positions shown by the tick marks at the top of each panel. The evaluated kinetic temperature $T^* \simeq$ 13 500 K is plotted in panel *a*.

Now comes the question about the most probable kinetic temperature and the accuracy of the approximation $n_e =$ constant. Table 2 shows the spread of the T_{kin} values between 13700 K and 18100 K for different models. Each of these models is acceptable from the statistical point of view. To select the adequate models additional observational data should be taken into account. For this purpose we consider below high SNR data on the unsaturated C IV and Si IV lines observed at the same $z =$ 2.504 towards Q1009+2956.

3   THE MEASUREMENT OF T_{kin} FROM METAL ABSORPTION LINES

We turn now to a brief discussion of the application of the entropy-regularized χ^2-minimization (ERM) procedure developed by Levshakov *et al.* (1999b, LTA hereinafter) to recover independently the kinetic temperature from the C IV and Si IV data obtained by BT. We suppose that H I and metals from the same Lyman limit system should give similar T_{kin}.

The ERM procedure utilizes complex but similar absorption line profiles of different ions to estimate a single value of T_{kin} for the whole absorbing region. The similarity of the complex profiles of ions with different masses and ionization potentials stems from the homogeneous gas density distribution along the sight-line, otherwise we would expect to observe different intensity fluctuations within the line profiles caused by variations of the local ionization parameter U (the ratio of
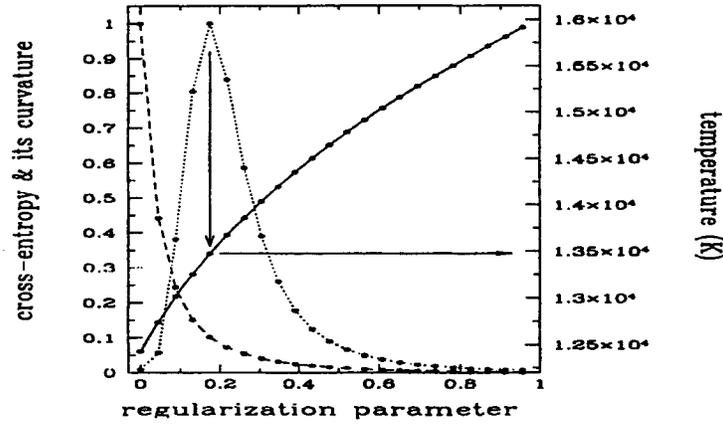
Figure 4 An example of the entropy-regularized χ^2-minimization (ERM) technique used to measure the kinetic temperature from the complex absorption spectra of the C IV and Si IV lines shown in Figure 3. The filled circles connected by dotted line show the normalized values of the cross-entropy $\hat{\mathcal{K}}$ as a function of the normalized regularization parameter $\hat{\alpha}$. The dashed curve is the normalized curvature of the $\hat{\mathcal{K}}(\hat{\alpha})$ trajectory. Its maximum at point $\hat{\alpha} = 0.174$ corresponds to the kinetic temperature $T^* \simeq 13\,500$ K which is indicated by arrows. For more details (especially on the ERM technique) the reader is encouraged to consult LTA.

the number of photons with energies above one Rydberg to the number of atoms, $U = n_\gamma/n_{\mathrm{gas}}$). If, however, we observe similar profiles and the gas density does vary, the ERM procedure yields the density weighted mean temperature (Levshakov and Kegel, 1999):

$$\langle T \rangle = \frac{\int n_{\mathrm{ion}}(s)T(s)\,\mathrm{d}s}{\int n_{\mathrm{ion}}(s)\,\mathrm{d}s}. \tag{6}$$

The absorber in question is the outer part of the halo of a distant galaxy. The gas in the halo photo-ionized by QSOs is optically thin in the Lyman continuum. For such system the equilibrium temperature is weakly dependent on U in the range $-4.7 \lesssim \log U \lesssim -1.8$ (see DS) and hence a single T_{kin} may be a suitable approximation.

To estimate T_{kin} for the particular $z = 2.504$ system, we have chosen C IVλ1548 (SNR $= 72$) and Si IVλ1394 (SNR $= 73$) lines observed with 8 km s^{-1} spectral resolution (FWHM) by BT. We did not use the red components of these doublets because their data are more noisy. Applying the ERM procedure to the C IVλ1548 and Si IVλ1394 lines, we obtained the gas temperature $T_{\mathrm{kin}}^* \simeq 13\,500$ K.

Figures 3 and 4 illustrate our results. The best-fitting profiles with three equidispersion components (for definition see Eq. (12) in LTA) are shown in panels a and b of Figure 3 by solid lines with the tick marks indicating the positions for the separate components. The choice of the appropriate $T_{\mathrm{kin}}^* \simeq 13\,500$ K corresponding to the optimal value of the normalized regularization parameter $\hat{\alpha}_{\mathrm{opt}} = 0.174$ is shown

in Figure 4. The objective function used in this case has the form

$$\mathcal{L}_\alpha = \chi^2 + \alpha\psi, \tag{7}$$

where ψ is a penalty function (Eq. (21) in LTA) and the regularization parameter α is given by

$$\alpha = \alpha_{min} + \hat{\alpha}(\alpha_{max} - \alpha_{min}). \tag{8}$$

For this particular case $\alpha_{min} = -0.19$ and $\alpha_{max} = 0.05$ were chosen.

The obtained ERM estimation of $T^*_{kin} \simeq 13\,500$ K lies in the range of T_{kin} found by the RMC method from the H+D Lyα and higher-order Lyman series profiles. Since the accuracy of the ERM solutions is shown to be about 10% (LTA, Levshakov and Kegel, 1999), models (a), (e), and (g) in Table 2 seem to be consistent with the ERM result. However, we cannot reject models (b), (c), (d), and (f) because one pair of lines (C IV and Si IV) cannot provide a warrant value of T_{kin}. It will be interesting to see if the red components of the C IV and Si IV doublets observed with higher signal-to-noise ratio give the same T_{kin}.

4   CONCLUSION

We have shown that the mesoturbulent model can explain the data adequately. In the following we discuss the relationship between the micro- and mesoturbulence models, and related issues.

The mesoturbulent model assumes constant T_{kin} and n_e but allows velocity correlations, while the microturbulent model allows different but constant T_{kin} and n_e for each of a finite number of components and assumes no coherent structure in the velocity field.

In the microturbulent approach it is explicitly assumed that the radial velocities are normally distributed so that the line profile is uniquely determined every time. In contrast, in the mesoturbulent approach we do not make the assumption of a Gaussian distribution for the radial velocities. This leads in turn to the concepts of randomness and unpredictability in the line formation process. That is to say, the apparent b-parameters usually measured in high-resolution spectra may not be suitable to determine the true ratio σ_t/v_{th} which is used to estimate the relative importance of the non-thermal broadening (see Paper I, for details).

In the two approaches, the D/H ratios are found to be similar for the particular $z = 2.504$ system. However, microturbulent models yield slightly lower deuterium abundance and rather narrow range ($\simeq 15\%$) of its uncertainty. In the mesoturbulent solutions, although the total hydrogen column densities lie inside the range found by BT, the D/H values are less restricted because, in general, the radial-velocity distribution function $p(v)$ is not known *a priori*. Our analysis gives a certain range for N(H I)$_{tot}$ and D/H due to the finite signal-to-noise ratio and different $p(v)$ configurations. This is shown in Figure 5 where different 1σ-confidence regions for this pair of physical parameters are depicted for models (a), (e), and
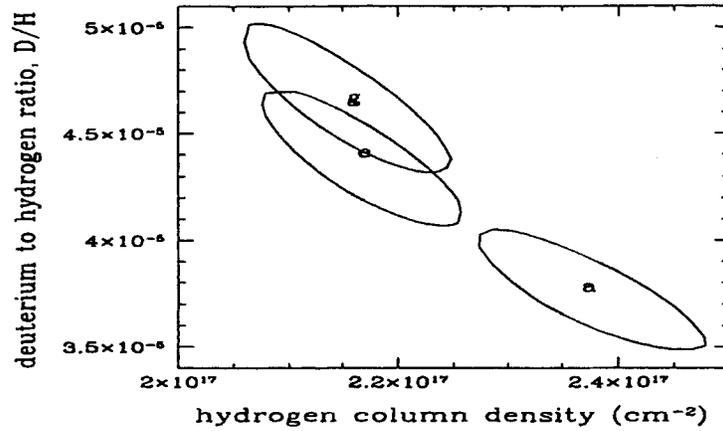
Figure 5 Confidence regions (68% confidence level) in the plane 'N(H I)–D/H' for solutions (a), (e), and (g) listed in Table 2. Different solutions give different contours. The other parameters of models (a), (e), and (g) – T_{kin}, σ_t/v_{th}, and L/l and the corresponding configurations of the velocity fields $v(s)$ are fixed. The size of the confidence region depends on signal to noise. The letters (a), (e), and (g) mark the points of maximum likelihood for models (a), (e), and (g) (see Table 2).

(g) under the assumption that the other parameters T_{kin}, σ_t/v_{th}, L/l and $v(s)$ are fixed (the computing procedure is described in Paper III).

The estimated D-abundance towards Q1009+2956 (D/H $\simeq$ 3.5–5.0 $\times$ 10^{-5}) agrees within the errors of measurement with the RMC results for the D I absorption systems seen towards Q1937–1009 (D/H $\simeq$ 3.8–4.8 $\times$ 10^{-5}: Levshakov *et al.*, 1998a) and towards Q1718+4807 (D/H $\simeq$ 3.0–7.5 $\times$ 10^{-5}: Levshakov *et al.*, 1998b; Levshakov, 1999).

The RMC calculations also reveal similar rms turbulent velocities and kinetic temperatures for all these systems yielding $\langle \sigma_t^* \rangle$ = 24 $\pm$ 5 km s^{-1} and $\langle T_{kin}^* \rangle$ = (15000 $\pm$ 2000) K, respectively. Mesoturbulent analysis shows that the observed velocity dispersions of the H and D lines are dominated by bulk motions, $\sigma_t/v_{th} \gtrsim 1$. We point out, however, that the same data being analyzed within the microturbulent approach give the opposite ratio $\sigma_t/v_{th} < 1$ (see BT). The mesoturbulent estimations lead every time to systematically lower T_{kin} and higher σ_t as compared with the microturbulent values. Fortunately, this uncertainty does not affect the D/H measurements since deuterium and hydrogen trace the same volume elements.

In general, accurate measurement of D/H requires (i) correct modelling, (ii) treatment of continuum placement errors reported by Burles and Tytler (1998a, 1998b), and (iii) treatment of contaminating absorption.

We conclude that the current observations support SBBN and that there is no conflict with the D/H measurements in these three Lyman limit systems. A single and robust value of D/H $\simeq$ 4 $\times$ 10^{-5} is sufficient to describe H+D profiles within

the framework of the mesoturbulent model.

Acknowledgements

References

Bechtold, J. and Ellingson, E. (1992) *Asrtophys. J.* **396**, 20.

Bergeron, J., Cristiani, S., and Shaver, P. (1992) *Astron. Astrophys.* **257**, 417.

Burles, S. and Tytler, D. (1998a) *Asrtophys. J.* **499**, 699.

Burles, S. and Tytler, D. (1998b) *Asrtophys. J.* **507**, 732 [BT].

Charlton, J. and Churchill, C. W. (1998) *Asrtophys. J.* **499**, 181.

Fixsen, D. J., Cheng, E. S., Gales, J. M., Mather, J. C., Shafer, R. A., and Wright, E. L. (1996) *Asrtophys. J.* **473**, 576.

Donahue, M. and Shull, J. M. (1991) *Asrtophys. J.* **383**, 511 [DS].

Jedamzik, K. anf Fuller, G. M. (1995) *Asrtophys. J.* **452**, 33.

Kurki-Suonio, H., Jedamzik, K., and Mathews, G. J. (1997) *Asrtophys. J.* **479**, 31.

Levshakov, S. A. (1999) In: *Proc. of the Xth Rencontres de Blois 'The Birth of Galaxies'* (22 June – 4 July, 1998, Blois, France), in press (astro-ph/9808295).

Levshakov, S. A. and Kegel, W. H. (1997) *Mon. Not. R. Astron. Soc.* **288**, 787 (Paper I).

Levshakov, S. A. and Kegel, W. H. (1999) In: *Proc. of the XIXth Moriond Astrophysics Meeting 'Building Galaxies: from the Primordial Universe to the Present'* (13–20 March, 1999, Les Arcs, France), in press (astro-ph/9905123).

Levshakov, S. A., Kegel, W. H., and Mazets, I. E. (1997) *Mon. Not. R. Astron. Soc.* **288**, 802 (Paper II).

Levshakov, S. A., Kegel, W. H., and Takahara, F. (1998a) *Asrtophys. J.* **499**, L1.

Levshakov, S. A., Kegel, W. H., and Takahara, F. (1998b) *Astron. Asrtophys.* **336**, L29.

Levshakov, S. A., Kegel, W. H., and Takahara, F. (1999a) *Mon. Not. R. Astron. Soc.* **302**, 707 (Paper III).

Levshakov, S. A., Takahara, F., and Agafonova, I. I. (1999b) *Asrtophys. J.* **517**, 609 (LTA).

Pettini, M., Kellogg, M., Steidel, C. C., Dickinson, M., Adelberger, K. L., and Giavalisco, M. (1998) *Asrtophys. J.* **508**, 539.

Schramm, D. N. (1998) In: N. Prantzos, M. Tosi, and R. von Steiger (eds.) *Primordial Nuclei and their Galactic Evolution*, Kluwer Academic, Dordrecht, The Netherlands, p. 3.

Tytler, D. and Burles, S. (1997) In: T. Kajino, Y. Yoshii, and S. Kubono (eds.) *Origin of Matter and Evolution of Galaxies*, World Scientific, Singapore, p. 37.

Tytler, D., Burles, S., Lu, L., Fan, X.-M., Wolfe, A., and Savage, B. D. (1998) *Asrton. J.* **117**, 63.

van Ojik, R., Röttgering, H. J. A., Miley, G. K., and Hunstead, R. W. (1997) *Astron. Astrophys.* **317**, 358.

Webb, J. K., Carswell, R. F., Lanzetta, K. M., Ferlet, R., Lemoine, M., Vidal-Madjar, A., and Bowen, D. V. (1997) *Nature* **388**, 250.